Molecular Dynamics Simulations Reveal a Disorder-to-Order Transition on Phosphorylation of Smooth Muscle Myosin

L. Michel Espinoza-Fonseca, David Kast, and David D. Thomas
Department of Biochemistry, Molecular Biology and Biophysics, University of Minnesota, Minneapolis, Minnesota 55455

ABSTRACT We have performed molecular dynamics simulations of the phosphorylated (at S-19) and the unphosphorylated 25-residue N-terminal phosphorylation domain of the regulatory light chain (RLC) of smooth muscle myosin to provide insight into the structural basis of regulation. This domain does not appear in any crystal structure, so these simulations were combined with site-directed spin labeling to define its structure and dynamics. Simulations were carried out in explicit water at 310 K, starting with an ideal α-helix. In the absence of phosphorylation, large portions of the domain (residues S-2 to K-11 and R-16 through Y-21) were metastable throughout the simulation, undergoing rapid transitions among α-helix, π-helix, and turn, whereas residues K-12 to Q-15 remained highly disordered, displaying a turn motif from 1 to 22.5 ns and a random coil pattern from 22.5 to 50 ns. Phosphorylation increased α-helical order dramatically in residues K-11 to A-17 but caused relatively little change in the immediate vicinity of the phosphorylation site (S-19). Phosphorylation also increased the overall dynamic stability, as evidenced by smaller temporal fluctuations in the root mean-square deviation. These results on the isolated phosphorylation domain, predicting a disorder-to-order transition induced by phosphorylation, are remarkably consistent with published experimental data involving site-directed spin labeling of the intact RLC bound to the two-headed heavy meromyosin. The simulations provide new insight into structural details not revealed by experiment, allowing us to propose a refined model for the mechanism by which phosphorylation affects the N-terminal domain of the RLC of smooth muscle myosin.

INTRODUCTION

Each muscle myosin (isoform II) molecule contains two heavy chains, and two pairs of associated calmodulin-like proteins called the essential light chain (ELC) and the regulatory light chain (RLC). The heavy chain is comprised of an N-terminal globular catalytic domain that contains both actin-binding and ATP-hydrolysis activities and an extended C-terminal α-helix that serves in dimerization and filament formation. Both the ELC and RLC are bound to this helical heavy chain region proximal to the N-terminus to form the light-chain domain (1) (Fig. 1).

In smooth muscle, phosphorylation of Thr-18 or Ser-19 on RLC by the Ca^{2+}/calmodulin-dependent myosin light chain kinase (MLCK) is required for activation of muscle contraction. The unphosphorylated state of smooth muscle myosin (SMM) has negligible catalytic activity, but phosphorylation produces as much as 1000-fold increase in actin-activated ATPase activity (2). This mechanism probably involves interactions between the two heads (S1) of myosin because heavy meromyosin (HMM), a fragment of myosin containing both heads and lacking the C-terminal two-thirds of the tail, is regulated (3,4), whereas both single-headed myosin (5,6) and S1 (7–9) are unregulated (constitutively active). More specifically, partial activation is achieved through relief of inhibitory interactions between the two unphosphorylated RLCs (10–12); full activation requires relief of additional inhibitory interactions involving one or both catalytic domains (13–16).

However, the structural basis of this regulatory mechanism remains unknown, in part because there is no crystal structure of a two-headed myosin fragment but primarily because there is no high-resolution structure of any myosin that includes the N-terminal portion of the RLC. For example, the crystal structure of skeletal S1 lacks the first 24 amino acids of the N-terminal region of the RLC, including the critical phosphorylation targets Thr-18 and Ser-19 (Fig. 1). Deletion and mutational studies in the N-terminus have identified additional residues, K-11 to R-16, as critical for changing the conformation of SMM and for activating the ATPase (17). Photo-cross-linking studies suggest that these residues must be disordered to allow the unphosphorylated N-terminus to interact with the partner RLC (10). Because only partial activation is caused by mutations that mimic the negative charge of phosphate (18), it is likely that phosphorylation produces a specific secondary structure change in these residues.

The most detailed information obtained to date on the structure of this N-terminal region of the RLC comes from recent solution electron paramagnetic resonance (EPR) studies, in which site-directed spin labeling was applied to RLC in HMM. A series of single-Cys RLC mutants was prepared, in which each of the N-terminal 25 residues (except for the phosphorylation sites, Thr-18 and Ser-19) was replaced by Cys, and EPR experiments were performed. The results showed that this N-terminal sequence acts as a distinct ''phosphorylation domain'', undergoing a substantial change

Submitted August 23, 2006, and accepted for publication January 11, 2007.

Address reprint requests to David D. Thomas, Dept. of Biochemistry, Molecular Biology and Biophysics, University of Minnesota, Minneapolis, MN 55455. E-mail: ddt@umn.edu.

Editor: David M. Warshaw.

0006-3495/07/09/2083/08 $2.00

doi: 10.1529/biophysj.106.095802

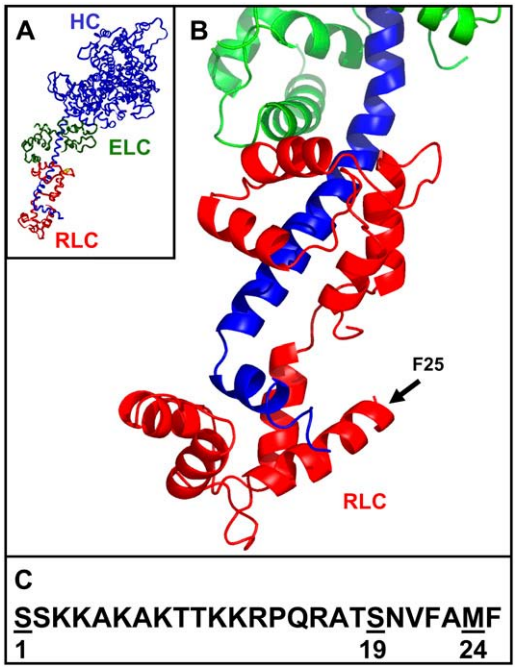

FIGURE 1 (*A*) Structure of myosin subfragment 1 (*1*). Blue, heavy chain; green, essential light chain; red, regulatory light chain (RLC). (*B*) Homology-modeled structure of smooth muscle myosin RLC. (*C*) N-terminal sequence of RLC (absent in crystal structure).

in side-chain mobility, solvent accessibility, and secondary structure on phosphorylation (19). Specifically, the unphosphorylated N-terminus is largely solvent inaccessible and only weakly helical, whereas the phosphorylated N-terminus exhibits substantially increased rotational mobility, solvent accessibility, and helical order. These results led to a model in which phosphorylation induces a disorder-to-order transition in the phosphorylation domain of RLC that removes the inhibitory head-head interaction (19).

However, these spectroscopic measurements did not provide high-resolution structural information, so there remains some ambiguity about the details of the phosphorylation-induced secondary structural transition. The study presented here uses molecular dynamics simulations to investigate the independent stability of the first 25 N-terminal residues of RLC in aqueous solvent. The results directly support previous experimental data and provide new physical insight into the nature of the disorder-to-order transition of the RLC N-terminal phosphorylation domain.

METHODS

Systems setup

The starting structure of the 25-residue N-terminal domain of the regulatory light chain of smooth muscle myosin of chicken gizzard was modeled as an ideal α-helix by using the program Swiss PDB Viewer (20). The sequence of the fragment is SSKKAKAKTTKKRPQRATSNVFAMF. Phosphorylation at S-19 was assigned with the aid of the PSFGEN utility, included in the latest version of the program NAMD (21). Both phosphorylated and unphosphorylated peptides were capped with an acetyl group at the N-terminus and *N*-methylamide at the C terminus, then embedded in a TIP3P water box with dimensions of 50 Å in each direction. Finally, eight- and six-Cl^- counterions were added to the systems containing the unphosphorylated and phosphorylated peptides, respectively. The latter procedure was employed to conserve the neutrality of the systems. An alternative approach, using $[Na^+Cl^-] \approx 0.15$ M, produced results that were not significantly different. All atoms were included, and the CHARMM22 force field was employed (22).

Molecular dynamics protocol

Simulations were performed using the NAMD 2.5 program (21). The NPT ensemble was used, with periodic boundary conditions (23). The electrostatic term was defined by using the particle mesh Ewald algorithm (24,25) with a grid size of 75 Å in each direction. The nonbonded cutoff, switching distance, and nonbonded pair-list distance were set to 8, 7, and 9.5 Å, respectively. The SHAKE (26) algorithm was applied for bonds involving hydrogen atoms, using a 2-fs time step. It has been shown that this use of the SHAKE algorithm reduces the computational cost by a factor of two without affecting the results obtained with a 1-fs time step (27). The impulse-based Verlet-I multi-step method was used with 2 fs for bonded, 4 fs short-range for nonbonded, and 8 fs for long-range electrostatic forces. Constant pressure (1 atm) and temperature (310 K) on the system were maintained with an isotropic Langevin barostat and a Langevin thermostat. These values of pressure and temperature were set to mimic the standard physiological conditions. Preliminary energy minimization was accomplished with 1000 steps of conjugate-gradient algorithm with restraints to the protein backbone, followed by 1000 steps without restraints. Systems were warmed up for 20 ps and equilibrated for 60 ps with lower restraints, finishing at no restraints and 310 K. Both simulations were continued for 50 ns of simulation. The simulations were run on an SGI Altix supercomputer at the Minnesota Supercomputing Institute.

Analysis and visualization

The Visual Molecular Dynamics (VMD) program (28) was used for analysis, visualization, and rendering of the structures. The program STRIDE (29), included in VMD, was used to analyze the evolution of the secondary structure of both phosphorylated and unphosphorylated peptides. STRIDE recognizes secondary structural elements in proteins from their atomic coordinates. It utilizes both hydrogen-bond energy and main-chain dihedral angles to define the secondary structure pattern. It relies on database-derived recognition parameters with the crystallographers' secondary structure definitions as a standard of truth.

RESULTS

The conformational evolution of the phosphorylated and unphosphorylated peptides was investigated by 50-ns simulations. The two peptides both showed dramatic structural fluctuations, which were affected by phosphorylation.

Fluctuations in secondary structure

The unphosphorylated peptide fragment (amino acids S-1 to A-24), maintains an α-helical pattern for only the first nanosecond (Fig. 2 *A*), after which time residues 12–15 and 21–24 spend the rest of the simulation fluctuating between coil and turn. Residues S-1 to K-11 and R-16 to N-20 keep the α-helical folding pattern until 5 ns. From 5 to 50 ns,

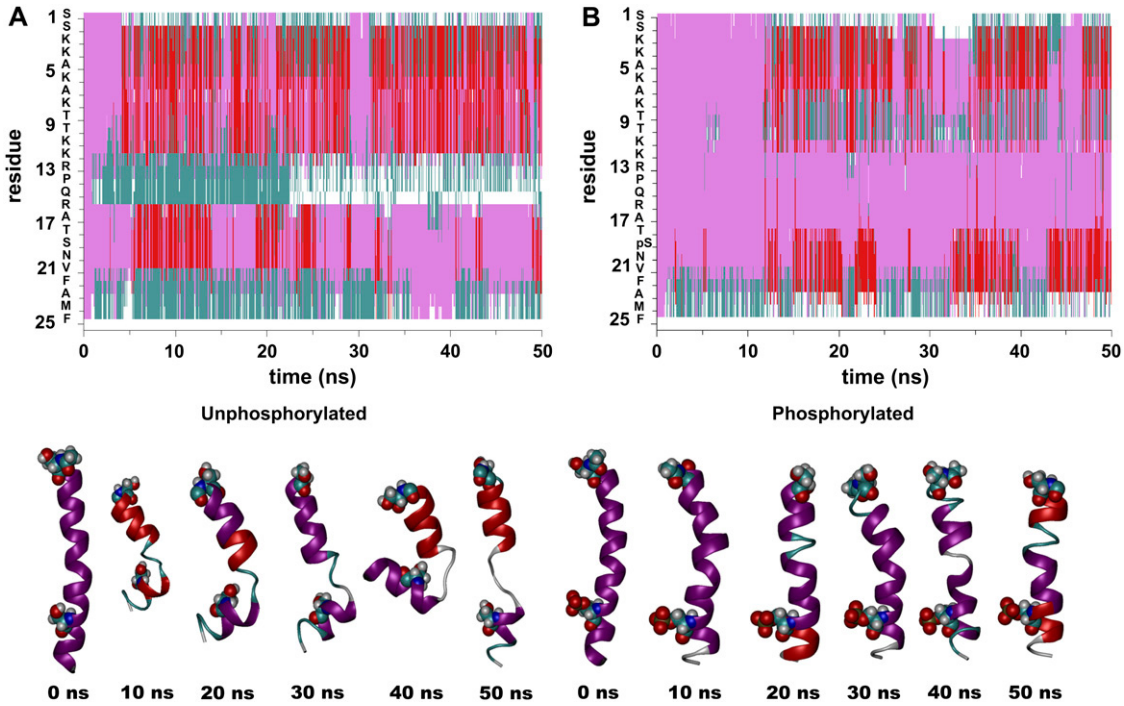

FIGURE 2 Evolution of the secondary structure of unphosphorylated (*A*) and phosphorylated (*B*) peptides along the 50-ns trajectory (*top*). Snapshots illustrating the key structural features are shown at bottom. The secondary structure is represented as ribbons, and atoms in residues S-1 and S-19 (pSer-S-19, *right*) are shown as van der Waals spheres. Secondary structure is colored as α-helix (*pink*), π-helix (*red*), turn (*cyan*), and coil (*white*).

residues S-2 to K-11 display an interesting pattern: the segment from S-2 to A-5 undergoes rapid (subnanosecond) transitions among α-helix, π-helix, and turn, whereas the segment from K-6 to K-11 shows rapid α-helix-to-π-helix transitions. The segment R-16 to N-20 (including the phosphorylation site at S-19) also begins fluctuating between α-helix and π-helix at ~5 ns but maintains a more α-helical pattern than does the amino-terminal segment. In summary, these MD simulations predict that the phosphorylation domain of RLC is highly flexible and dynamically unstable, undergoing subnanosecond fluctuations in secondary structure throughout its 25-residue sequence.

Phosphorylation induces a disorder-to-order transition

Phosphorylation causes dramatic changes in the trajectory (Fig. 2 *B*). The initial α-helical pattern remains stable over most of the peptide for a much longer period, over 10 ns instead of just 1 ns. The most striking change is that the central portion of the peptide (residues 12–19) remains α-helical throughout most of the 50-ns trajectory (Fig. 2 *B*), whereas this segment is predominantly random coil in the absence of phosphorylation (Fig. 2 *A*). These effects of phosphorylation are further illustrated by plots of the percentage of time spent by each amino acid in the α- and π-helical (Fig. 3) conformations. Phosphorylation increases α-helicity over much of the peptide, particularly in residues 11–17, and decreases π-helicity in residues 2–12. In contrast, in residues 18–24, α-helix decreases whereas π-helix increases. Remarkably, there is relatively little effect in the immediate vicinity of the phosphorylated residue, S-19, despite

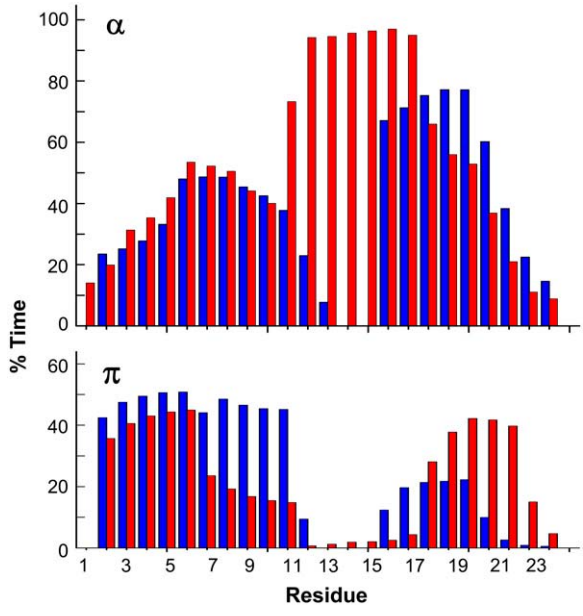

FIGURE 3 Percentage of time (after the first 12 ns) that each residue spends in α-helix (*top*) and π-helix (*bottom*) for unphosphorylated (*blue*) or phosphorylated (*red*) peptide.

large effects on the amino-terminal side of this residue (Figs. 2 and 3). Additional simulations were performed to make certain that the steady-state structures represented by Fig. 3 were not sensitive to arbitrary assumptions. For example, these results were not significantly affected by increasing the simulation time to 70 ns (i.e., the average ensemble of the trajectories displayed the same structural patterns), showing that these results represent an equilibrated system. Similarly, the results of Fig. 3 were not significantly affected by starting with a π-helix rather than α-helix.

Phosphorylation decreases the amplitude of structural fluctuations

Structural fluctuations were characterized further by the root mean-square deviation (RMSD) (Fig. 4). In the absence of phosphorylation (Fig. 4 *A*), a rapid global conformational change occurs in the first 3 ns, increasing the RMSD to ~5 Å. This conformational change is principally caused by the formation of the turn K-12 to Q-15 (Fig. 2 *A*). During the period between 4 and 22 ns, the RMSD plot shows good stability of the peptide's dynamics, with no large changes in RMSD. However, after $t \approx 23$ ns, several large transitions in RMSD are observed, covering a range from 3 to 8 Å, consistent with large-scale conformational changes. Thus, changes in the RMSD of 3–4 Å are observed at 34.3, 35.1, 35.4, 40.9, and 43.5. These rapid conformational changes appear to depend on the flexible nature of the unfolded fragment K-12 to Q-15.

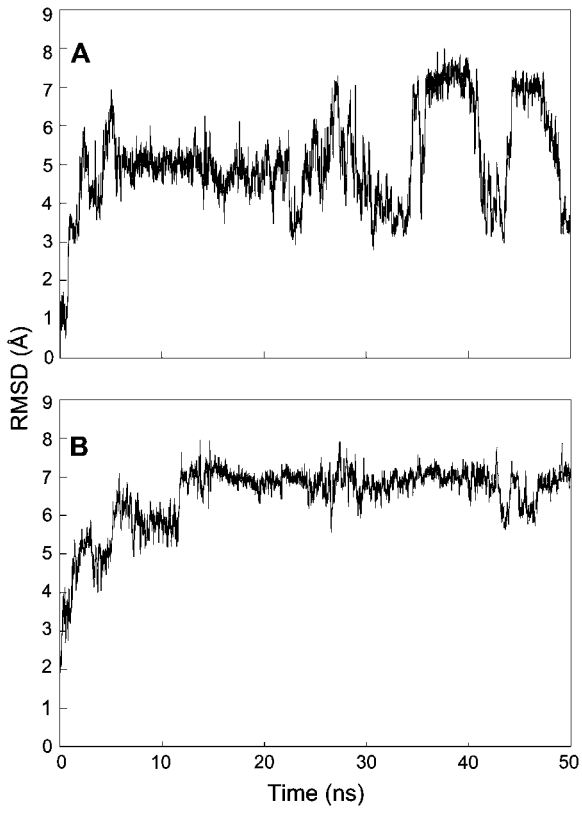

FIGURE 4 RMSD of the unphosphorylated (*A*) and phosphorylated (*B*) peptides throughout the 50-ns simulation.

Phosphorylation greatly increases the dynamic stability, as evidenced by decreased temporal fluctuation of the RMSD (Fig. 4 *B*). In this case, the RMSD shows a more gradual increase, not leveling off for ~12 ns. Although the RMSD remains at a higher level (~7 Å, Fig. 4 *B*) than in the absence of phosphorylation (~5 Å, Fig. 4 *A*), much smaller fluctuations are observed in the RMSD value (≤1 Å), indicating that only relatively small conformational changes are occurring that affect the global dynamics of the peptide.

DISCUSSION

Metastable secondary structure

One of the most striking features of the MD trajectory, in both phosphorylated and unphosphorylated peptides, is the lack of a stable secondary structure throughout most of the peptide sequence. Instead, the dominant motif is a rapidly fluctuating structure, involving subnanosecond transitions among α-helix, π-helix, and turn (Figs. 2 and 3). This is especially evident in segments 2–11 and 16–21. The π-helix, which is rarely seen in crystal structures, is characterized by an (i,i + 5) hydrogen-bonding pattern. This rarity (instability) is attributable to several factors, including unfavorable ϕ and ψ angles ($\phi = -76 \pm 25°$, $\psi = -41 \pm 24°$ (30,31)), a larger radius (4.4 residues per turn, 16 atoms in the ring closed by a hydrogen bond) than that of the α-helix (3.6 residues per turn, 13 atoms in the ring closed by a hydrogen bond), which results in unfavorable energetics in the helix core (32) and a large entropic cost required to align five residues in a helix to permit the hydrogen bond (33). Thus, it is not surprising that this motif is rarely seen in crystal structures, and it has been suggested that the presence of a stable π-helix in MD simulations may sometimes result from deficiencies in the force fields used in those simulations (34). However, the existence of a metastable π-helix, rapidly interconverting with α-helix as observed in the study presented here, has been observed in MD simulations on model peptides (35) and a highly charged region of caldesmon (36).

Secondary structure prediction, using a multiple alignment-based neural network system (37), suggests that residues K-3 to K-11 are likely to form an α-helix; our simulations do indicate a predominantly helical structure, but one that is dynamic and metastable. This decreased stability and increased dynamics probably arise in part from the electrostatic repulsion caused by the large positive charge, including eight positively charged residues N-terminal to the phosphorylatable serine. This concentration of basic residues has been shown to be favorable for interactions with myosin light chain kinase (38), and it may also play a role in ensuring that kinase substrates tend to be dynamic and metastable (39).

Influence of phosphorylation at S-19

As mentioned in Results, important differences in the structure and dynamics of the phosphorylated and unphosphorylated fragments were observed. The region comprising residues K-11 through A-17 undergoes the most dramatic change. In the unphosphorylated peptide, this region shows very little secondary structural order, probably because of the well-known helix-breaking property of proline, which is found at position 14. In the simulation, this region rapidly changes into a turn and subsequently into a random coil (Fig. 2). In contrast, phosphorylation at S-19 preserves the α-helix through a salt bridge or hydrogen bond with the R-16 side chain (Fig. 5). This interaction changes the Q-15 dihedral angles from the β-sheet region to the α-helical region on the Ramachandran plot (Fig. 6). Meanwhile, the proline dihedral angle distribution becomes slightly more helical, without any loss in helicity of K-12 and R-13. However, the cost of ordering the K-12 through Q-15 region is increased helix-turn fluctuations over residues 7–11 (Fig. 2 *B*).

The dramatic ordering effect of phosphorylation is illustrated by the decreased fluctuations in the RMSD (Fig. 4) but also in the calculated root mean-square fluctuations (Fig. 7). In this case, residues K-12 to A-17 present a difference $\geq$2 Å. Consequently, we conclude that the effect of phosphorylation in the N-terminal domain of RLC is not simply to reduce the net positive charge; rather, it serves as a structural switch, increasing both the helical content and dynamic stability.

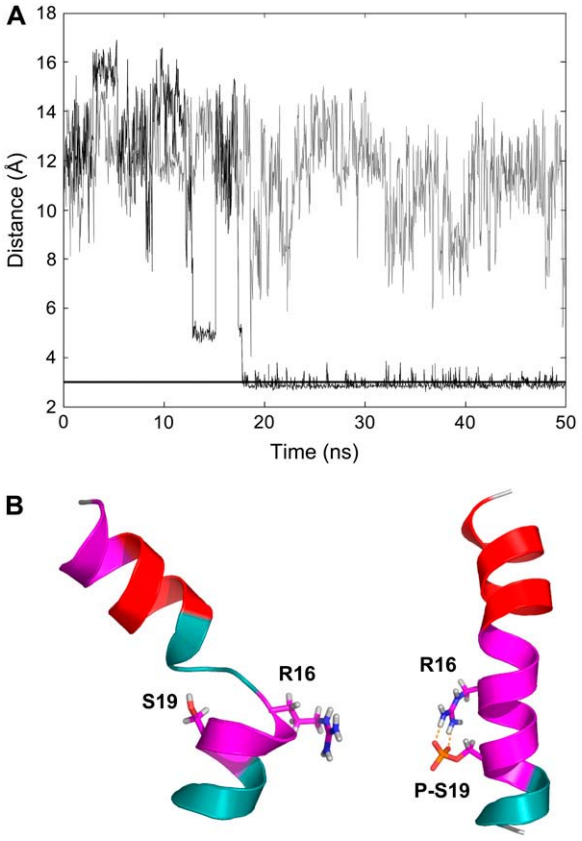

FIGURE 5 (*A*) Average distance between R-16 side-chain amino protons with serine hydroxyl (*gray*) or phosphoserine oxygens (*black*). After 19 ns, R-16 amino protons interact with P-S-19 through a salt bridge or hydrogen bond. (*B*) Representative snapshots of the unphosphorylated (*left*) and phosphorylated (*right*) N-terminal peptides with the same color scheme as in Fig. 2.

Relationship to experimental data

The structure of the 25-amino-acid N-terminal phosphorylation domain (PD) of the RLC of smooth muscle myosin has not been solved by crystallography, but considerable information about the structure and dynamics of this region has been provided by site-directed spin labeling (19). That EPR study on spin-labeled RLC, functionally bound to myosin HMM, showed that this region indeed acts as a domain in that phosphorylation globally increases the side-chain mobility and accessibility in this entire region without exerting similar effects on the rest of the RLC. The pattern of accessibility along the sequence indicated clearly that α-helical periodicity increases with phosphorylation. In this study, we report a computational model for structural dynamics of this region, as affected by phosphorylation. Although these molecular dynamics simulations made no assumptions based on the EPR study, the results of the simulations are in remarkable agreement with most aspects of the EPR data: phosphorylation increases helical content, especially in the central region of this domain (Figs. 2 and 3) and increases dynamic stability (Figs. 4 *B* and 7).

The experimental and computational data are complementary. Because of computational limitations, this study was limited to the 25-residue PD, isolated in solution, whereas the EPR study was carried out on the fully functional two-headed HMM molecule. The agreement between the two approaches indicates that the structural dynamics of this domain is, to a first approximation, determined by its sequence, independently of the rest of the protein. In addition, the MD simulations go well beyond the EPR data to define the currently most reliable model for the atomic structure and dynamics of the RLC and its stabilization on phosphorylation, as discussed above. For example, the ambiguity of α-helical periodicity in the EPR data in regions S-1 through T-9 and T-18 through M-24 (19) is clarified by the MD simulations, which show that these regions are metastable, undergoing rapid structural fluctuations, regardless of phosphorylation (Fig. 2). Thus, rather than a transition from disorder to complete order, the observed transition might be more precisely described as a partial ordering of a metastable domain.

This study, limited to the phosphorylation domain of the RLC, clearly does not provide a full explanation of the mechanism of SMM regulation, which has been proposed to involve changes in head-head interactions (10,11,13–15). Indeed, those few aspects of the experimental EPR observations of Nelson et al. (19) that are not confirmed by our simulations on the isolated peptide (e.g., global increases in

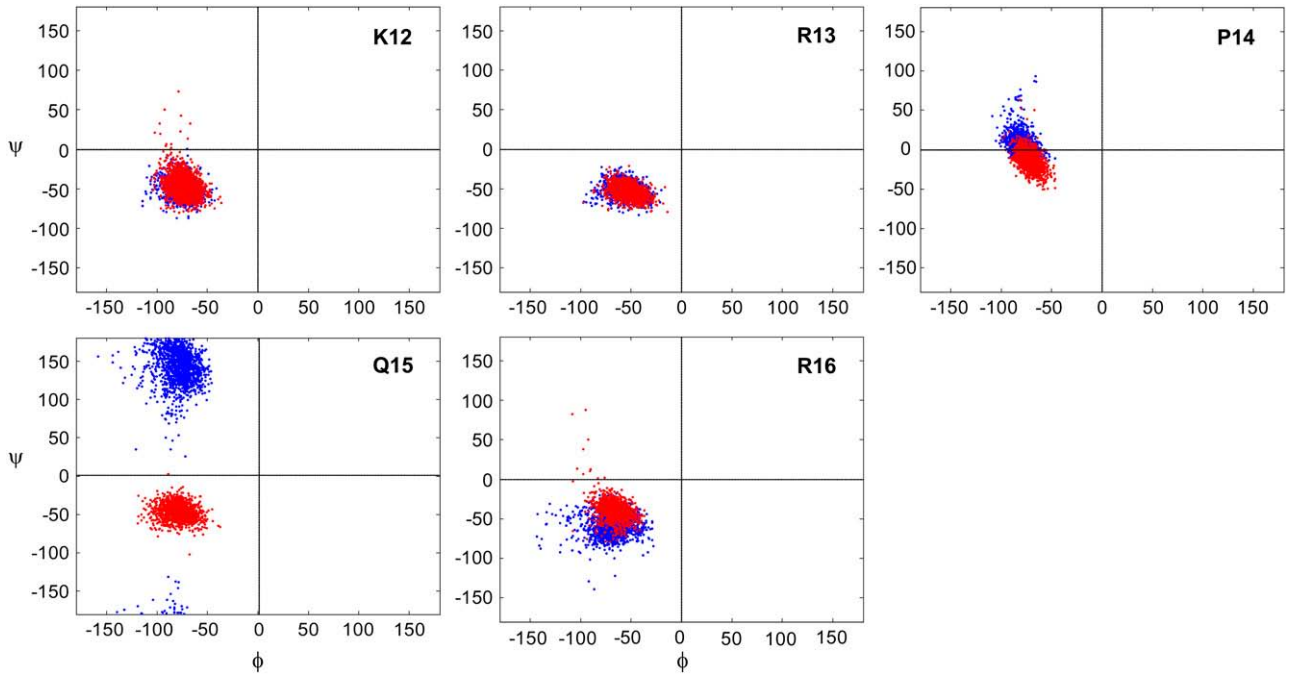

FIGURE 6 Ramachandran (ϕ,ψ) plots of unphosphorylated (*blue*) and phosphorylated (*red*) residues that demonstrate the largest helical change in Fig. 3.

solvent accessibility and dynamics as a result of phosphorylation) are easily explained by decreased head-head interactions on phosphorylation (19). Clearly, further testing of more complete models of SMM regulation, such as the blocked motor domain model proposed by electron cryomicroscopy of frozen hydrated unphosphorylated HMM (15), will require more extensive spectroscopic and computational studies of the entire HMM molecule.

Other studies on the structural dynamics of phosphorylation

MD simulations in other proteins and peptides have predicted both ordering and disordering effects on phosphorylation in different systems (40,41). Smart and McCammon employed hybrid Monte Carlo/stochastic dynamics on a polyalanine peptide capped with phosphoserine at the N-terminus and found that phosphorylation stabilizes the helix via simple electrostatic interactions (42). Experimental data on other systems also indicate that both global ordering (43) and disordering (44) events can accompany regulatory phosphorylation (45).

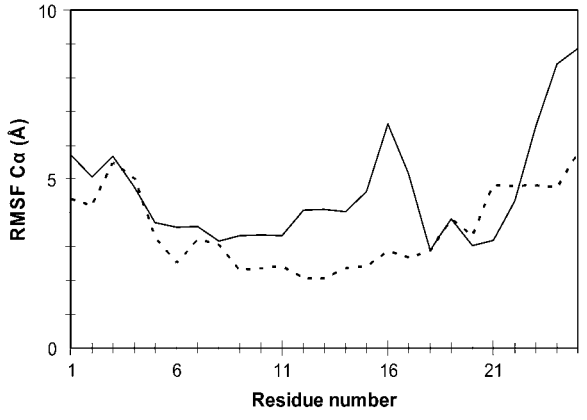

FIGURE 7 Calculated root-mean-square fluctuations of the α-carbons of both unphosphorylated (*solid line*) and phosphorylated (*dashed line*) fragment.

The only previous case in which the effects of phosphorylation on dynamics were studied by both experiment and MD simulation was that of phospholamban (PLB), a 52-residue membrane-spanning protein that regulates the membrane-bound sarcoplasmic reticulum Ca-ATPase (SERCA). Inhibition is accomplished through transmembrane domain interactions between PLB and SERCA and is relieved by phosphorylation at S-16 in the cytoplasmic domain of PLB. Both magnetic resonance experiments (46–48) and MD simulations (49) demonstrate that PLB undergoes an order-to-disorder transition in which the loop between S-16 and P-21 becomes destabilized on phosphorylation, leading to further destabilization of the N-terminal helix. Phosphate introduces a salt bridge between R-13 and the phosphoserine, moving both residues from the α-helical region to the β-sheet region of a Ramachandran plot. This results in residues R-9 through A-15, N-terminal of the loop, to spend $\sim$50% less time in a helical conformation.

Analogously, the side chain of RLC N-terminus R-16 forms a salt bridge with P-S-19, located three residues C-terminal to R-16 (Fig. 5), and forces neighboring residues (especially Q-15) dihedral angles from the β-sheet region to the α-helical region (Fig. 3). In contrast to PLB, this results

in a large increase in the time spent in the helical conformation. Although the PLB (order-to-disorder) and RLC (disorder-to-order) examples appear to be opposite, in one sense they are quite similar—in both cases, it is the less helical, more dynamically disordered conformation of the peptide that interacts more strongly with its regulatory target. In one case (RLC) this interaction leads to inhibition (19); in the other case (PLB) it leads to activation (47,49). In both cases, the unphosphorylated proteins are metastable, fluctuating between ordered and dynamically disordered structures, so that the phosphorylation event encounters only a small energetic barrier to shift the conformational switch. These constitute the most compelling experimental and computational results yet obtained in support of the proposal that regulatory signaling and energy transduction, whether by phosphorylation or other means, harness the conformational and energetic advantages of dynamic disorder (39,47,50).

CONCLUSIONS

In this study, we have used MD simulations to explore the effect of phosphorylation on the N-terminal phosphorylation domain of the regulatory light chain of smooth muscle myosin. Our results are in good agreement with complementary experimental data (19), defining a phosphorylation-induced disorder-to-order transition, and provide new insight into the structural dynamics of this protein domain. Simulations confirm that the unphosphorylated domain is dynamically disordered but show that most of it is not found as a random coil. Rather, a large portion (at both ends) of the domain is metastable, undergoing subnanosecond α-helix/π-helix/turn transitions in both phosphorylated and unphosphorylated proteins. In contrast, the dynamics and structural stability of a small central region of the domain are highly dependent on phosphorylation. Phosphorylation at S-19 causes a dramatic disorder-to-order transition in residues 11–17, converting a dynamically unstructured region to a stable α-helix, accompanied by formation of a salt bridge between the phosphoserine and R-16. This mechanism produces an efficient conformational switch that ultimately activates myosin's interaction with actin, possibly by decreasing head-head interactions (19). These observations help to explain how the function of myosin is regulated. More generally, this study adds to the evidence that the regulation of dynamic disorder is involved in key processes of biological regulation and energy transduction (39,47).

We thank Dr. Wendy Nelson for fruitful discussions and facilitating the analysis of her EPR data.

This work was supported by grants to D.D.T. from the National Institutes of Health (AR32961). D.K. was supported by the National Institutes of Health/National Institute of Arthritis and Musculoskeletal and Skin Diseases Training Program for Muscle Research (T32 AR07612) and the Victor Bloomfield Fellowship for Biophysics. We are grateful for the resources provided by the University of Minnesota Supercomputing Institute.

REFERENCES

1. Rayment, I., W. R. Rypniewski, K. Schmidt-Base, R. Smith, D. R. Tomchick, M. M. Benning, D. A. Winkelmann, G. Wesenberg, and H. M. Holden. 1993. Three-dimensional structure of myosin subfragment-1: a molecular motor. *Science.* 261:50–58.
2. Sellers, J. R. 1985. Mechanism of the phosphorylation-dependent regulation of smooth muscle heavy meromyosin. *J. Biol. Chem.* 260:15815–15819.
3. Sellers, J. R. 1991. Regulation of cytoplasmic and smooth muscle myosin. *Curr. Opin. Cell Biol.* 3:98–104.
4. Ellison, P. A., J. R. Sellers, and C. R. Cremo. 2000. Kinetics of smooth muscle heavy meromyosin with one thiophosphorylated head. *J. Biol. Chem.* 275:15142–15151.
5. Cremo, C. R., J. R. Sellers, and K. C. Facemyer. 1995. Two heads are required for phosphorylation-dependent regulation of smooth muscle myosin. *J. Biol. Chem.* 270:2171–2175.
6. Sata, M., M. Matsuura, and M. Ikebe. 1996. Characterization of the motor and enzymatic properties of smooth muscle long S1 and short HMM: role of the two-headed structure on the activity and regulation of the myosin motor. *Biochemistry.* 35:11113–11118.
7. Sellers, J. R., M. D. Pato, and R. S. Adelstein. 1981. Reversible phosphorylation of smooth muscle myosin, heavy meromyosin, and platelet myosin. *J. Biol. Chem.* 256:13137–13142.
8. Konishi, K., S. Kojima, T. Katoh, M. Yazawa, K. Kato, K. Fujiwara, and H. Onishi. 2001. Two new modes of smooth muscle myosin regulation by the interaction between the two regulatory light chains, and by the S2 domain. *J. Biochem. (Tokyo).* 129:365–372.
9. Ikebe, M., and D. J. Hartshorne. 1985. Proteolysis of smooth muscle myosin by *Staphylococcus aureus* protease: preparation of heavy meromyosin and subfragment 1 with intact 20 000-dalton light chains. *Biochemistry.* 24:2380–2387.
10. Wahlstrom, J. L., M. A. Randall Jr., J. D. Lawson, D. E. Lyons, W. F. Siems, G. J. Crouch, R. Barr, K. C. Facemyer, and C. R. Cremo. 2003. Structural model of the regulatory domain of smooth muscle heavy meromyosin. *J. Biol. Chem.* 278:5123–5131.
11. Wu, X., B. A. Clack, G. Zhi, J. T. Stull, and C. R. Cremo. 1999. Phosphorylation-dependent structural changes in the regulatory light chain domain of smooth muscle heavy meromyosin. *J. Biol. Chem.* 274:20328–20335.
12. Li, X. D., J. Saito, R. Ikebe, K. Mabuchi, and M. Ikebe. 2000. The interaction between the regulatory light chain domains on two heads is critical for regulation of smooth muscle myosin. *Biochemistry.* 39:2254–2260.
13. Rovner, A. S., P. M. Fagnant, and K. M. Trybus. 2006. Phosphorylation of a single head of smooth muscle myosin activates the whole molecule. *Biochemistry.* 45:5280–5289.
14. Li, X. D., and M. Ikebe. 2003. Two functional heads are required for full activation of smooth muscle myosin. *J. Biol. Chem.* 278:29435–29441.
15. Wendt, T., D. Taylor, K. M. Trybus, and K. Taylor. 2001. Three-dimensional image reconstruction of dephosphorylated smooth muscle heavy meromyosin reveals asymmetry in the interaction between myosin heads and placement of subfragment 2. *Proc. Natl. Acad. Sci. USA.* 98:4361–4366.
16. Sweeney, H. L., L. Q. Chen, and K. M. Trybus. 2000. Regulation of asymmetric smooth muscle myosin II molecules. *J. Biol. Chem.* 275:41273–41277.
17. Ikebe, M., R. Ikebe, H. Kamisoyama, S. Reardon, J. P. Schwonek, C. R. Sanders 2nd, and M. Matsuura. 1994. Function of the NH_2-terminal domain of the regulatory light chain on the regulation of smooth muscle myosin. *J. Biol. Chem.* 269:28173–28180.
18. Sweeney, H. L., Z. Yang, G. Zhi, J. T. Stull, and K. M. Trybus. 1994. Charge replacement near the phosphorylatable serine of the myosin regulatory light chain mimics aspects of phosphorylation. *Proc. Natl. Acad. Sci. USA.* 91:1490–1494.
19. Nelson, W. D., S. E. Blakely, Y. E. Nesmelov, and D. D. Thomas. 2005. Site-directed spin labeling reveals a conformational switch in the

phosphorylation domain of smooth muscle myosin. *Proc. Natl. Acad. Sci. USA.* 102:4000–4005.

20. Guex, N., and M. C. Peitsch. 1997. SWISS-MODEL and the Swiss-PdbViewer: an environment for comparative protein modeling. *Electrophoresis.* 18:2714–2723.
21. Kale, L., R. Skeel, M. Bhandarkar, R. Brunner, A. Gursoy, N. Krawetz, J. Phillips, A. Shinozaki, K. Varadarajan, and K. Schulten. 1999. NAMD2: Greater scalability for parallel molecular dynamics. *J. Comput. Phys.* 151:283–312.
22. MacKerell, A. D., Jr., D. Bashford, M. Bellott, R. L. Dunbrack Jr., J. D. Evanseck, M. J. Field, S. Fischer, J. Gao, H. Guo, S. Ha, D. Joseph-McCarthy, L. Kuchnir, K. Kuczera, F. T. K. Lau, C. Mattos, S. Michnick, T. Ngo, D. T. Nguyen, B. Prodhom, W. E. Reiher III, B. Roux, M. Schlenkrich, J. C. Smith, R. Stote, J. Straub, M. Watanabe, J. Wiorkiewicz-Kuczera, D. Yin, and M. Karplus. 1998. All-atom empirical potential for molecular modeling and dynamics studies of proteins. *J. Phys, Chem. B* 102:3586–3616.
23. Weber, W., P. H. Hünenberger, and J. A. McCammon. 2000. Molecular dynamics simulations of a polyalanine octapeptide under Ewald boundary conditions: influence of artificial periodicity on peptide conformation. *J. Phys. Chem. B.* 104:3668–3675.
24. Darden, T., D. York, and L. Pedersen. 1993. Particle mesh Ewald: An $N\cdot\log(N)$ method for Ewald sums in large systems. *J. Chem. Phys.* 98:10089–10092.
25. Essmann, U., L. Perera, and M. L. Berkowitz. 1995. A smooth particle mesh Ewald method. *J. Chem. Phys.* 103:8577–8593.
26. van Gunsteren, W. F., and H. J. C. Berendsen. 1977. Algorithms for macromolecular dynamics and constraint dynamics. *Mol. Phys.* 34: 1311–1327.
27. Adcock, S. A., and J. A. McCammon. 2006. Molecular dynamics: survey of methods for simulating the activity of proteins. *Chem. Rev.* 106:1589–1615.
28. Humphrey, W., A. Dalke, and K. Schulten. 1996. VMD: Visual Molecular Dynamics. *J. Mol. Graph.* 14:33–38, 27–28.
29. Frishman, D., and P. Argos. 1995. Knowledge-based protein secondary structure assignment. *Proteins.* 23:566–579.
30. Ramachandran, G. N., and V. Sasisekharan. 1968. Conformation of polypeptides and proteins. *Adv. Protein Chem.* 23:283–438.
31. Fodje, M. N., and S. Al-Karadaghi. 2002. Occurrence, conformational features and amino acid propensities for the pi-helix. *Protein Eng.* 15:353–358.
32. Low, B. W., and R. B. Baybutt. 1952. The pi-helix—a hydrogen bonded configuration of the polypeptide chain. *Protein Sci.* 5:1687–1696.
33. Rohl, C. A., and A. J. Doig. 1996. Models for the 3(10)-helix/coil, pi-helix/coil, and alpha-helix/3(10)-helix/coil transitions in isolated peptides. *Protein Sci.* 5:1687–1696.
34. Feig, M., A. D. MacKerell Jr., and C. L. Brooks III. 2003. Force field influence on the observation of pi-Helical protein structures in molecular dynamics simulations. *J. Phys. Chem. B* 107:2831–2836.
35. Lee, K. H., D. R. Benson, and K. Kuczera. 2000. Transitions from alpha to pi helix observed in molecular dynamics simulations of synthetic peptides. *Biochemistry.* 39:13737–13747.
36. Shepherd, C. M., D. van der Spoel, and H. J. Vogel. 2004. Molecular dynamics simulations of peptides from the central domain of smooth muscle caldesmon. *J. Biomol. Struct. Dyn.* 21:555–566.
37. Rost, B., J. Liu, R. Nair, K. O. Wrzeszczynski, and Y. Ofran. 2003. Automatic prediction of protein function. *Cell. Mol. Life Sci.* 60:2637–2650.
38. Kemp, B. E., and R. B. Pearson. 1990. Protein kinase recognition sequence motifs. *Trends Biochem. Sci.* 15:342–346.
39. Iakoucheva, L. M., P. Radivojac, C. J. Brown, T. R. O'Connor, J. G. Sikes, Z. Obradovic, and A. K. Dunker. 2004. The importance of intrinsic disorder for protein phosphorylation. *Nucleic Acids Res.* 32:1037–1049.
40. Groban, E. S., A. Narayanan, and M. P. Jacobson. 2006. Conformational changes in protein loops and helices induced by post-translational phosphorylation. *PLoS Comput. Biol.* 2:e32.
41. Hamelberg, D., T. Shen, and J. A. McCammon. 2005. Phosphorylation effects on *cis*/*trans* isomerization and the backbone conformation of serine-proline motifs: accelerated molecular dynamics analysis. *J. Am. Chem. Soc.* 127:1969–1974.
42. Smart, J. L., and J. A. McCammon. 1999. Phosphorylation stabilizes the N-termini of alpha-helices. *Biopolymers.* 49:225–233.
43. Yang, J., P. Cron, V. Thompson, V. M. Good, D. Hess, B. A. Hemmings, and D. Barford. 2002. Molecular mechanism for the regulation of protein kinase B/Akt by hydrophobic motif phosphorylation. *Mol. Cell.* 9:1227–1240.
44. Steinmetz, M. O., W. Jahnke, H. Towbin, C. Garcia-Echeverria, H. Voshol, D. Muller, and J. van Oostrum. 2001. Phosphorylation disrupts the central helix in Op18/stathmin and suppresses binding to tubulin. *EMBO Rep.* 2:505–510.
45. Johnson, L. N., and R. J. Lewis. 2001. Structural basis for control by phosphorylation. *Chem. Rev.* 101:2209–2242.
46. Metcalfe, E. E., N. J. Traaseth, and G. Veglia. 2005. Serine 16 phosphorylation induces an order-to-disorder transition in monomeric phospholamban. *Biochemistry.* 44:4386–4396.
47. Karim, C. B., Z. Zhang, E. C. Howard, K. D. Torgersen, and D. D. Thomas. 2006. Phosphorylation-dependent conformational switch in spin-labeled phospholamban bound to SERCA. *J. Mol. Biol.* 358:1032–1040.
48. Traaseth, N. J., D. D. Thomas, and G. Veglia. 2006. Effects of Ser16 phosphorylation on the allosteric transitions of phospholamban/Ca(2+)-ATPase complex. *J. Mol. Biol.* 358:1041–1050.
49. Paterlini, M. G., and D. D. Thomas. 2005. The alpha-helical propensity of the cytoplasmic domain of phospholamban: a molecular dynamics simulation of the effect of phosphorylation and mutation. *Biophys. J.* 88:3243–3251.
50. Thomas, D. D., S. Ramachandran, O. Roopnarine, D. W. Hayden, and E. M. Ostap. 1995. The mechanism of force generation in myosin: a disorder-to-order transition, coupled to internal structural changes. *Biophys. J.* 68:135S–141S.